AI assisted design of ligands for Lipocalin-2

Jacopo Sgrignani[1*†], Sara Buscarini[1†], Patrizia Locatelli[1], Concetta Guerra[1], Alberto Furlan[1], Yingyi Chen[1], Giada Zoppi[1], and Andrea Cavalli[1,2]*

1 Institute for Research in Biomedicine (IRB), Università della Svizzera Italiana (USI), Via Chiesa 5, 6500, Bellinzona (CH).

2 Swiss Institute of Bioinformatics (SIB), Lausanne, Switzerland.

*Corresponding authors:

Dr. Andrea Cavalli

Institute for research in Biomedicine (IRB)

Universita' della Svizzera Italiana (USI)

Via Chiesa 5, 6500 Bellinzona (CH)

Dr. Jacopo Sgrignani

Institute for research in Biomedicine (IRB)

Universita' della Svizzera Italiana (USI)

Via Chiesa 5, 6500 Bellinzona (CH)

† These authors share first authorship.

Abstract

Lipocalin-2 (LCN2) is an acute-phase glycoprotein whose up-regulation correlates with blood–brain-barrier breakdown and neuro-inflammatory damage, making it an attractive diagnostic and therapeutic target. Here we present an end-to-end, AI-guided workflow that rapidly generates de-novo miniproteins able to bind LCN2. Backbone scaffolds were generated with RFdiffusion, sequences were optimized with ProteinMPNN, and candidates filtered in silico using a consensus score based on AlphaFold2 confidence scores (mean interface pAE < 10) and interaction free energy calculated by Prodigy before experimental screening. From 10,000 designed sequences, five were expressed and purified from *E. coli*. Biolayer interferometry (BLI) identified a lead construct, MinP-2, that bound to LCN2 with dissociation constant of K_d = 0.7 nM. Furthermore, structural modeling suggests that binding is primarily mediated by hydrogen bonds between backbone elements. These findings demonstrate that a fully computational generative pipeline can deliver nanomolar LCN2 binders in a single design–build–test cycle. MinP-2 offers a promising starting point for affinity maturation, structural elucidation, and in-vivo evaluation as an imaging probe or antagonist of LCN2-mediated signaling.

Introduction

Lipocalin-2 (LCN2) is an acute-phase glycoprotein (also known as neutrophil gelatinase-associated lipocalin, siderocalin or 24p3) that is rapidly up-regulated during infection, sterile inflammation (Chandrasekaran et al., 2024).

Like other members of the lipocalin family, LCN2 adopts the canonical eight-stranded β-barrel, which allows it to bind bacterial siderophores and sequester iron, thereby acting as a key first-line defense mechanism against pathogens (Fig. 1) (Chia et al., 2011;Chandrasekaran et al., 2024).

The interaction between LCN2 and its receptor LCN2 receptor (LCN2R/NGALR) plays a significant role in various cellular processes and has been implicated in several pathological conditions. In particular, it has been demonstrated that binding to NGALR amplifies pro-inflammatory cytokine release (Jha et al., 2015;Shao et al., 2016) and, when over-expressed by reactive glia, contributes to neurotoxicity in multiple central nervous system (CNS) disorders (Afridi et al., 2024).

Several studies (Triebel et al., 1992;Kjeldsen et al., 1993) have shown that LCN2 can form heterodimers with MMP-9, a zinc-dependent metalloproteinase from the matrixin family. This interaction stabilizes MMP-9, preventing its degradation. MMP-9 plays a critical role in breaking down extracellular matrix components. Excessive MMP-9 activity can disrupt the integrity of the Blood-Brain Barrier (BBB), contributing to the development of neurodegenerative diseases such as Alzheimer's and Parkinson's (Jung and Ryu, 2023). Additionally, dysregulation of MMP-9 has been linked to various pathological conditions, including ischemia, trauma, neurodegenerative disorders (Ram et al., 2006) (Shigemori et al., 2006) and brain tumors (Vafadari et al., 2016).

Despite the central role of lipocalin-2 (LCN2) in neuroinflammation, no ligands currently exist that can efficiently cross the blood–brain barrier (BBB) and either block the LCN2–

NGALR signaling axis or disrupt the LCN2–MMP-9 heterodimer, both of which represent promising therapeutic strategies. Current approaches to mitigate LCN2-mediated pathogenic mechanisms include reducing its transcription or secretion, promoting its degradation, employing neutralizing antibodies to attenuate its biological activity, using antagonists to block receptor interactions, or inhibiting downstream receptor signaling. Among small-molecule-based strategies, promising results have been reported for the proteasome inhibitor bortezomib, which reduces LCN2 transcription, and for the autophagy activator Torin 1, which lowers LCN2 protein levels (Qiu et al., 2024). Antibody-based therapies also represent a potentially effective approach to block LCN2 function and signaling. However, due to their large molecular weight, the use of antibodies in neurological diseases is limited by poor BBB permeability. To overcome these challenges, we hypothesized that an engineered miniprotein binder with high affinity for LCN2 could serve as a versatile and BBB-compatible platform for therapeutic intervention. Currently, protein-protein interaction (PPI) modulators are categorized based on their characteristics into small molecules, peptides, and antibodies (Nada et al., 2024). While small molecules offer advantages such as improved absorption and stability, peptides and antibodies are often more effective at disrupting PPIs, particularly those involving large, flat interaction interfaces that lack well-defined binding pockets.

Recently, multiple groups - most prominently the Baker laboratory - released artificial intelligence (AI) tools that enable in-silico generation of small proteins (10-15 kDa) binding a protein of interest, commonly referred to as miniproteins (Cao et al., 2020b;Huang et al., 2024;Weinberg et al., 2024;Yang et al., 2025).

Inspired by these advances, we applied an AI-guided pipeline to generate de-novo miniproteins that occlude the LCN2 interfaces used by NGALR and MMP-9.

Here we report the design, recombinant production using *E. coli* and biophysical characterisation of five candidates, culminating in a lead miniprotein with nanomolar affinity for LCN2.

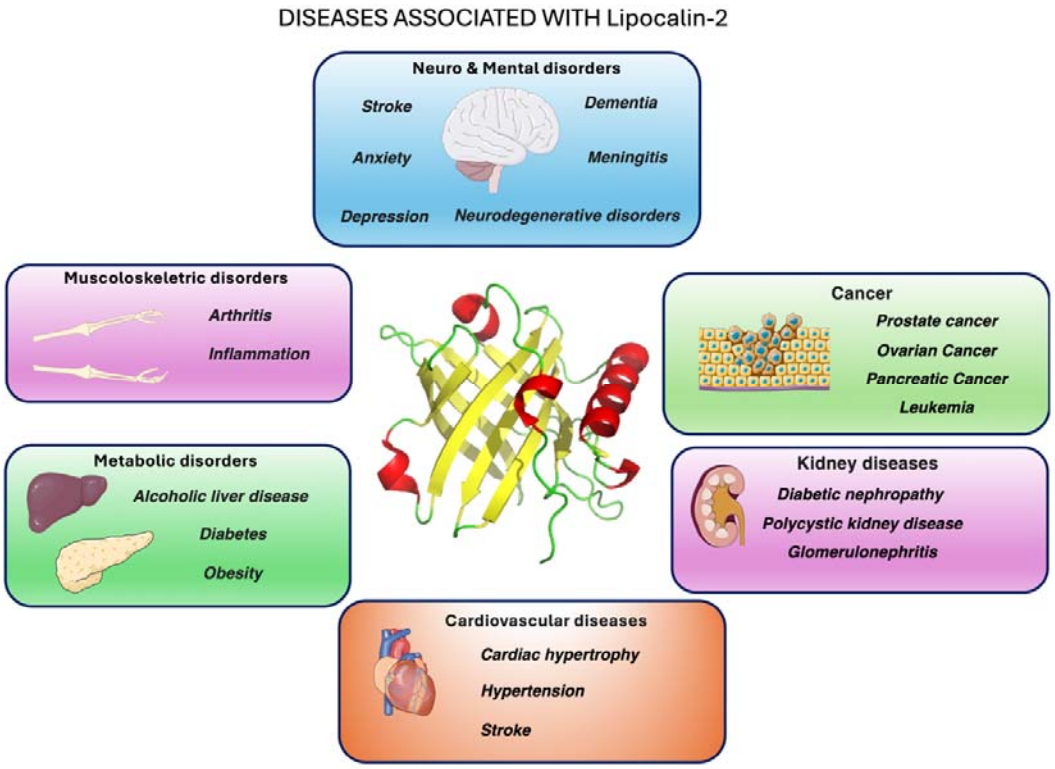

Figure 1. Graphical overview of major pathological conditions linked to LCN2 (lipocalin-2, also known as neutrophil gelatinase-associated lipocalin, siderocalin or 24p3) overexpression or activity. At the center, the X-ray crystal structure of human LCN2 (PDB ID: 3FW4; Bao et al., 2010) is shown, with secondary structure elements highlighted: α-helices in red, β-strands in blue, and loops in green.

Methods

General reagents and buffers

All chemicals were analytical grade. Recombinant human LCN2 was produced and purified by GenScript. Twin-Strep–tag magnetic beads, Buffer W and Buffer BXT were from IBA LifeSciences. Dynamic-light-scattering (DLS) and nano-DSF assays were carried out in phosphate-buffered saline (PBS; 20 mM sodium-phosphate, 150 mM NaCl, pH 7.4). All other solutions are described below.

Miniprotein computational design

The generation of mini proteins to bind LCN2 was carried out using the procedure described by Baker and co-workers (Watson et al., 2023). (https://github.com/RosettaCommons/RFdiffusion). Firstly, the atomistic structure of LCN2 deposited under PDB 1DFV was selected as template structure (Goetz et al., 2000). Following the protocol author's suggestion, we first generated 10,000 scaffolds using RF diffusion (Watson et al., 2023) and subsequently designed 10,000 sequences with ProteinMPNN (Dauparas et al., 2022) to create LCN2 binders. Finally, the ability of the generated sequences to correctly fold and to bind the target was evaluated using AlphaFold2 (AF2) (Jumper et al., 2021).

For each model we recorded the mean pLDDT and the interface predicted aligned-error (pAE_interface). Designs were retained when pAE_interface<10, yielding 1,184 candidates.

Next, to select the five most promising binders to express and purify we estimated the affinity between LCN2 and all the selected binders using PRODIGY, a contact-based predictor of protein-protein affinity (Vangone and Bonvin, 2017). Finally, the five proteins reporting the most negative ΔG were expressed and purified.

Assessment of protein expression

The DNA sequences encoding the five select miniproteins were synthetized and cloned by GenScript into the pET30b plasmid, incorporating a Twin-Strep tag for purification. *E. coli* BL21 (DE3) pLysS cells were transformed with the plasmids and plated onto five separate LB-agar plates. Following overnight incubation, colonies that successfully incorporated the plasmids were selected.

Before starting the protein production and purification, we assessed miniprotein expression in E.coli BL21 (DE3) pLysS cells analyzing induced and not induced cultures by Western-Blot (WB).

20 µl of both IPTG-induced and non-induced samples were mixed with 20 µl of Sample Buffer containing Tris-Glycine SDS and a Sample Reducing Agent. From these prepared stocks, 20 µl were loaded onto the gel. Following electrophoresis, the SDS-PAGE gel was transferred into a membrane. After the transfer, the membrane was activated with methanol and subsequently washed with Tris-buffered saline containing 0. 1% Tween® 20 (TBST). Following the washing step, blocking was performed with TBST and milk to prevent nonspecific binding. Subsequently, another washing step was conducted, and the primary antibody (IBA Lifesciences 2-1507-001; Anti-Strep) was added.

The next day, the primary antibody was removed, and the secondary antibody (anti-mouse IgG1 conjugated with horseradish peroxidase (HRP)) was applied. After the incubation step, another washings step was performed, and reagents were added to develop the Western Blot.

Miniprotein expression and purification

Considering the positive feedback about the protein expression given by WB analysis, a bacterial preculture was prepared by inoculating a single colony into 7 mL of Luria-Bertani

(LB) medium supplemented with chloramphenicol and kanamycin. The culture was incubated at 37°C to promote bacterial growth.

Subsequently, 1 mL of the preculture was inoculated into 200 mL of LB medium and incubated at 37 °C until the culture reached an OD of 0.6. Protein expression was then induced by adding IPTG to a final concentration of 1 mM.. After overnight incubation, bacterial cells were resuspended in a PBS addicted with two tablets of protease inhibitor (cOmplete™, Mini, EDTA-free Protease Inhibitor Cocktail) and lysed by sonication. The lysate was then filtered through a 0.22 µm membrane to remove debris before purification.

For purification, Strep-tag technology was employed using magnetic beads (IBA LifeSciences). The beads were washed with 1X Buffer W, followed by an incubation step to allow protein binding. After additional washing, elution was carried out using 1X Buffer BXT, yielding purified miniproteins in the eluate.

To assess purification efficiency, SDS-PAGE analysis was performed. Finally, biotin present in the elution buffer was removed by dialysis.

Dynamic-light scattering (DLS) and nano-DSF

To assess the size distribution and thermal stability, all miniproteins were analyzed using a Prometheus Panta instrument (NanoTemper). Measurements were performed in triplicate, with miniproteins directly loaded into capillaries at concentrations of 0.32, 0.22, 0.18, 0.10, and 0.2 mg/mL for MinP-1, MinP-2, MinP-3, MinP-4, and MinP-5, respectively.

Bio-layer interferometry (BLI)

The interaction between the designed miniproteins and LCN2 was evaluated using biolayer interferometry (BLI). LCN2 was immobilized by His-tag on BLI sensors Octet® Ni-NTA (NTA) Biosensors using a concentration of 5µg/ml. All the experiments were run using a

Octet® R8 instrument. As preliminary screening all the miniproteins were tested at a concentration of 4 μM. Subsequently, MinP-2 for which we detected a clear binding was characterized performing a titration with different concentrations, namely 1000, 500, 250, 125, 62.5, 31.2 and 15.6 nM. The signal from a reference sensor without the immobilized protein was subtracted from all other sensors to remove background noise and account for nonspecific binding. Association and dissociation phases were 300 and 300 s each; data were fitted globally with a 1:1 binding model in the Octet Analysis software.

Results

In-silico miniprotein design pipeline and candidate selection

In the initial phase of the project, we applied the computational pipeline originally proposed by Baker and colleagues (Watson et al., 2023). Starting from 10,000 backbone scaffolds generated with RFdiffusion, a single ProteinMPNN sequence was designed for each scaffold. AlphaFold2 rescoring retained 1,184 binders with a pAE_interaction score below 10 - a threshold shown to enrich for functional hits (Bennett et al., 2023).

However, expressing and purifying such a large number of proteins remains impractical. To overcome this limitation, we applied a consensus scoring approach to refine the selection. Specifically, all 1,184 candidates were re-ranked with the contact-based affinity predictor PRODIGY, a contact-based predictor of protein-protein affinity (Vangone and Bonvin, 2017), and the five miniproteins (Figure 2B-F) with the most negative predicted ΔG were selected for expression (Table 1).

Table 1. Aminoacidic sequences and predicted ΔG for the five miniproteins selected for further studies after computational design. The ligands are ordered by pae_interaction score.

Name	**Sequence**	**Predicted ΔG (kcal/mol)**	**Pae_interactition**
MinP-1	KKKVAVVVVRKTPEEAKAGFEEAKPNVELVASILSEDFEVETLAVTEEEYDEVLEKYDFVVRVYKMDLESAKISAKLIREHIKEIVK	-11.0	4.05
MinP-2	MSKATVYDVSTGKTYEVSLEDAKKLASYAVYEGGYPLRISVAPEDTKAILDAIKNTSKEKAEEGKKLLEELN	-12.7	4.08
MinP-3	MKRVEIKALDNVENANAIAEVLKSHGIPVEVKEVSPDLKEVTSEAVVSEELAEKIKESLIELAKKLGPVGPIHISISDV	-11.7	4.20
MinP-4	MTVNVTITANSDGWISIKATTDETAKLAVEIAKEYLPTKSFDETAEATINALATKKGGTATITKSGNTYYATIT	-13.4	4.22
MinP-5	MLKELEEKIFKENPEVKKLLEKLSKALGVKVEVSVEKVDGVYRFVLRVDVKDHPKVNMKILSELGLKLQLAAGEELTKLL	-12.3	4.22

Expression, purification and biophysical characterization of AI designed miniproteins

Given that the proteins were designed by AI, before proceeding to large-scale production we assessed the expression of five constructs in *E. coli* by WB (Figure S1). This preliminary analysis confirmed that all proteins were expressed in bacteria, although MinP-2 and MinP-3 exhibited lower expression levels. Consequently, we proceeded with the expression and purification of all five constructs on a larger scale. Purification was carried out using magnetic beads functionalized with a modified version of streptavidin (Strep-Tactin®XT, IBA Lifesciences). The final purification yielded highly pure proteins in sufficient quantities for subsequent biophysical characterization of the modules (Figure S2).

Before assessing the ability of the AI-generated proteins to bind LCN2, we characterized all purified constructs in terms of size distribution using Dynamic Light Scattering (DLS) and thermal stability using nanoDSF. DLS analysis revealed that all constructs, except MinP-4, were monodisperse with an estimated hydrodynamic radius of approximately 2 nm—consistent with their predicted molecular weight and structural models (Figure S3). In

contrast, MinP-4 exhibited a polydispersity index (PDI) of 0.38, indicative of aggregation. Thermal stability analysis by nanoDSF showed that only MinP-5 displayed a clear melting temperature (Tm at 46.8 °C. This is notably lower than the high thermal stability (Tm > 90 °C) reported for some AI-designed miniprotein binders by Baker and colleagues (Cao et al., 2020a).

Binding of miniproteins to LCN2 investigated by BLI

Preliminary experiments at a concentration of 4 μM were carried out to assess the ability of the five miniproteins to effectively bind LCN2. These experiments indicated MinP-2 as the more promising binders for lipocalin (Figure 3H), while the other four ligands show poor or no bidning to the target.

Therefore, aimed to fully characterized the affinity and kinetics of the LCN2/MinP-2 binding we carried out a titration using 7 different concentrations. This experiment indicated that this miniprotein is able to strongly bind LCN2 being the two Kd values determined fitting the experimental data using a 2:1 heterogeneous model Kd1 = 0.7 and Kd2 = 35 nM, respectively.

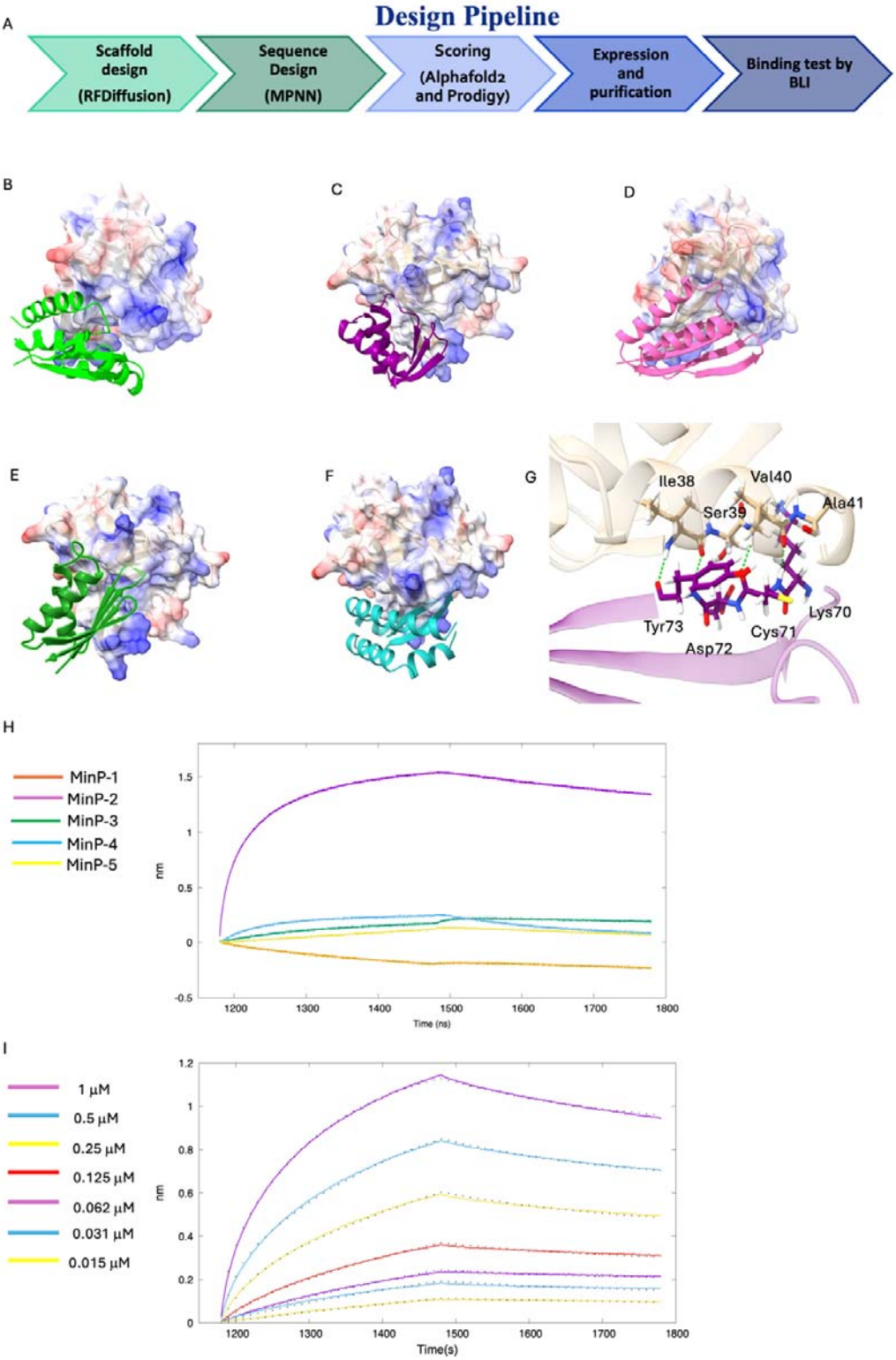
A
Design Pipeline
Scaffold design (RFDiffusion)
Sequence Design (MPNN)
Scoring (Alphafold2 and Prodigy)
Expression and purification
Binding test by BLI
B
C
D
E
F
G
Ile38
Val40
Ser39
Ala41
Lys70
Tyr73
Cys71
Asp72
H
MinP-1
MinP-2
MinP-3
MinP-4
MinP-5
nm
Time (ns)
I
1 μM
0.5 μM
0.25 μM
0.125 μM
0.062 μM
0.031 μM
0.015 μM
nm
Time(s)

Figure 2. (A) Schematic representation of the applied computational pipeline. (B-F) predicted structures of the complexes formed between LCN2 and the five selected miniproteins, as generated by AlphaFold2. (G) Key molecular interactions driving the binding of MinP-2 (magenta cartoons) to LCN2 (white cartoons). (H) Preliminary BLI analysis of miniprotein binding to LCN2 at a fixed concentration of 4 μM. Color coding: MinP-1 (orange), MinP-2 (violet), MinP-3 (green), MinP-4 (light blue), MinP-5 (yellow). (I) BLI titration experiment assessing the binding affinity of Mod-2 to LCN2 across seven concentrations, from top to bottom: 1 μM (violet), 0.5 μM (light blue), 0.25 μM (yellow), 0.125 μM (red), 0.625 μM (violet), 0.312 μM (light blue), and 0.156 μM (yellow). Experimental binding curves are shown as colored lines; corresponding fitted values are indicated by black dots.

Structural insight into the LCN2/MinP-2 interface

AlphaFold2 models predict that binding is dominated by backbone hydrogen bonds between LCN2 residues Lys70−Tyr73 and MinP-2 residues Ile38−Ala41, forming a short antiparallel β-augmentation interface (Figure 3G). Side-chain contacts from MinP-2 residues Val30 and Tyr49 further stabilize the complex, rationalizing the observed low-nanomolar affinity.

Discussion

Among other effects, Lipocalin-2 (LCN2) drives blood–brain barrier (BBB) breakdown and neuroinflammation through interactions with its partners NGALR and MMP-9; however, no ligands smaller than antibodies are currently available to block these interactions. Here we show that a 12-kDa miniprotein (MinP-2) generated in a single AI-guided cycle binds LCN2 with low-nanomolar affinity (KD 0.7 nM), representing >20-fold higher affinity than the best

reported siderophore mimetics and approaching that of monoclonal antibodies while retaining a 10-fold smaller molecular weight.

Our strategy, incorporating a contact-based scoring approach, demonstrates that consensus rescoring with AlphaFold2 and PRODIGY can enrich true positives to a practical experimental set. All five selected miniproteins were successfully expressed in *E. coli*, and four were monodisperse and thermostable.

In fact, quality control analyses performed using DLS and nanoDSF revealed that, with the exception of MinP-5, all proteins are thermally stable and predominantly monomeric in PBS at a concentration of ~10–12 μM, consistent with previous reports (Vázquez Torres et al., 2024). However, MinP-4 exhibited a tendency toward aggregation, representing an exception to this general behavior.

BLI experiments showed that all designed miniproteins were binding LCN2. Among them, MinP-2 showed the most promising interaction and was therefore selected for in-depth characterization. Binding analysis revealed that MinP-2 interacts with LCN2 with a dissociation constant (Kd) of 0.7 nM, highlighting its potential for future applications in therapeutic or diagnostic settings.

To better understand MinP-2's binding mode, we examined AlphaFold2 models of the LCN2 MinP-2 complex. The analysis indicates that affinity is dominated by a short β-augmentation segment: backbone-to-backbone hydrogen bonds form between LCN2 residues Lys70−Tyr73 and MinP-2 residues Ile38−Ala41, creating a continuous eight-strand sheet that anchors the miniprotein to its target.

Aiming to verify the potential ability of MinP-2 to block the interaction with MMP-9 and NGALR, we predicted the structure of the complexes between LCN2 and these two proteins by AlphaFold3. The output of these calculations (Fig. 4) indicated that MinP-2 has the potentiality to hinder their interaction with LCN2.

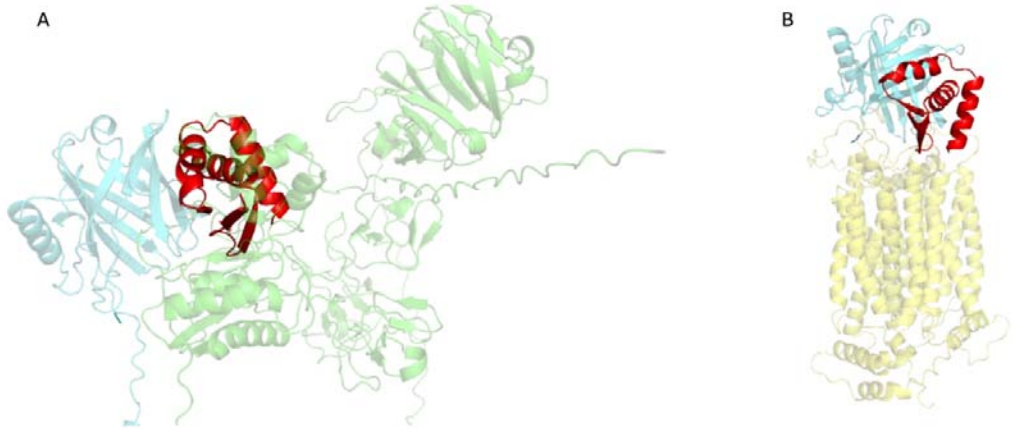

Figure 3. (A) Atomistic models of the LCN2 (acquamarine)-MMP-9 (green) complex displayed together with the structure of MinP-2 (red). (B) Atomistic models of the LCN2 (acquamarine)-NGALR (yellow) complex displayed together with the structure of MinP-2 (red).

Conclusions

In this work, we demonstrated that a fully automated, AI-driven workflow—RFdiffusion for backbone creation, ProteinMPNN for sequence optimisation, and AlphaFold2 for structure-based triage—can deliver potent miniproteins against LCN2.

From an initial library of 10,000 in-silico designs, five candidates were produced recombinantly, and one (MinP-2) bound LCN2 with high affinity while retaining excellent solubility and thermal stability. Furthermore, structural models suggest that binding is dominated by a short antiparallel β-augmentation interface, a motif that could be grafted onto alternative scaffolds.

These findings establish a starting point for developing LCN2-targeted diagnostics or therapeutics that modulate neuro-inflammatory pathways. Future work will focus on (i) solving a high-resolution structure of the MinP-2–LCN2 complex and (ii) evaluating the miniprotein's capacity to disrupt pathological LCN2 interactions in cellular and *in-vivo* models. More broadly, our study reinforces the utility of generative deep-learning methods to accelerate ligand discovery for challenging protein–protein interfaces, even in the absence of prior binder templates.

Founding

This work was supported by the SNF grant CRSII—222762**.**

Bibliography

Afridi, R., Kim, J.H., Bhusal, A., Lee, W.H., and Suk, K. (2024). Lipocalin-2 as a mediator of neuroimmune communication. *J Leukoc Biol* 116**,** 357-368.

Bennett, N.R., Coventry, B., Goreshnik, I., Huang, B., Allen, A., Vafeados, D., Peng, Y.P., Dauparas, J., Baek, M., Stewart, L., Dimaio, F., De Munck, S., Savvides, S.N., and Baker, D. (2023). Improving de novo protein binder design with deep learning. *Nat Commun* 14**,** 2625.

Cao, L., Goreshnik, I., Coventry, B., Case, J.B., Miller, L., Kozodoy, L., Chen, R.E., Carter, L., Walls, A.C., Park, Y.-J., Strauch, E.-M., Stewart, L., Diamond, M.S., Veesler, D., and Baker, D. (2020a). De novo design of picomolar SARS-CoV-2 miniprotein inhibitors. *Science (New York, N.Y.)* 370**,** 426-431.

Cao, L., Goreshnik, I., Coventry, B., Case, J.B., Miller, L., Kozodoy, L., Chen, R.E., Carter, L., Walls, A.C., Park, Y.J., Strauch, E.M., Stewart, L., Diamond, M.S., Veesler, D., and Baker, D. (2020b). De novo design of picomolar SARS-CoV-2 miniprotein inhibitors. *Science (New York, N.Y.)* 370**,** 426-431.

Chandrasekaran, P., Weiskirchen, S., and Weiskirchen, R. (2024). Structure, Functions, and Implications of Selected Lipocalins in Human Disease. *International journal of molecular sciences* 25**,** 4290.

Chia, W.J., Dawe, G.S., and Ong, W.Y. (2011). Expression and localization of the iron-siderophore binding protein lipocalin 2 in the normal rat brain and after kainate-induced excitotoxicity. *Neurochem Int* 59**,** 591-599.

Dauparas, J., Anishchenko, I., Bennett, N., Bai, H., Ragotte, R.J., Milles, L.F., Wicky, B.I.M., Courbet, A., De Haas, R.J., Bethel, N., Leung, P.J.Y., Huddy, T.F., Pellock, S., Tischer, D., Chan, F., Koepnick, B., Nguyen, H., Kang, A., Sankaran, B., Bera, A.K., King, N.P., and Baker, D. (2022). Robust deep learning-based protein sequence design using ProteinMPNN. *Science (New York, N.Y.)* 378**,** 49-56.

Huang, B., Coventry, B., Borowska, M.T., Arhontoulis, D.C., Exposit, M., Abedi, M., Jude, K.M., Halabiya, S.F., Allen, A., Cordray, C., Goreshnik, I., Ahlrichs, M., Chan, S., Tunggal, H., Dewitt, M., Hyams, N., Carter, L., Stewart, L., Fuller, D.H., Mei, Y., Garcia, K.C., and Baker, D. (2024). De novo design of miniprotein antagonists of cytokine storm inducers. *Nat Commun* 15**,** 7064.

Jha, M.K., Lee, S., Park, D.H., Kook, H., Park, K.G., Lee, I.K., and Suk, K. (2015). Diverse functional roles of lipocalin-2 in the central nervous system. *Neurosci Biobehav Rev* 49**,** 135-156.

Jumper, J., Evans, R., Pritzel, A., Green, T., Figurnov, M., Ronneberger, O., Tunyasuvunakool, K., Bates, R., Žídek, A., Potapenko, A., Bridgland, A., Meyer, C., Kohl, S.a.A., Ballard, A.J., Cowie, A., Romera-Paredes, B., Nikolov, S., Jain, R., Adler, J., Back, T., Petersen, S., Reiman, D., Clancy, E., Zielinski, M., Steinegger, M., Pacholska, M., Berghammer, T., Bodenstein, S., Silver, D., Vinyals, O., Senior, A.W., Kavukcuoglu, K., Kohli, P., and Hassabis, D. (2021). Highly accurate protein structure prediction with AlphaFold. *Nature* 596**,** 583-589.

Jung, B.K., and Ryu, K.Y. (2023). Lipocalin-2: a therapeutic target to overcome neurodegenerative diseases by regulating reactive astrogliosis. *Exp Mol Med* 55**,** 2138-2146.

Nada, H., Choi, Y., Kim, S., Jeong, K.S., Meanwell, N.A., and Lee, K. (2024). New insights into protein-protein interaction modulators in drug discovery and therapeutic advance. *Signal Transduct Target Ther* 9**,** 341.

Qiu, R., Cai, Y., Su, Y., Fan, K., Sun, Z., and Zhang, Y. (2024). Emerging insights into Lipocalin-2: Unraveling its role in Parkinson's Disease. *Biomedicine & Pharmacotherapy* 177**,** 116947.

Ram, M., Sherer, Y., and Shoenfeld, Y. (2006). Matrix metalloproteinase-9 and autoimmune diseases. *J Clin Immunol* 26**,** 299-307.

Shao, S., Cao, T., Jin, L., Li, B., Fang, H., Zhang, J., Zhang, Y., Hu, J., and Wang, G. (2016). Increased Lipocalin-2 Contributes to the Pathogenesis of Psoriasis by Modulating Neutrophil Chemotaxis and Cytokine Secretion. *J Invest Dermatol* 136**,** 1418-1428.

Shigemori, Y., Katayama, Y., Mori, T., Maeda, T., and Kawamata, T. (2006). Matrix metalloproteinase-9 is associated with blood-brain barrier opening and brain edema formation after cortical contusion in rats. *Acta Neurochir Suppl* 96**,** 130-133.

Vafadari, B., Salamian, A., and Kaczmarek, L. (2016). MMP-9 in translation: from molecule to brain physiology, pathology, and therapy. *Journal of Neurochemistry* 139**,** 91-114.

Vangone, A., and Bonvin, A. (2017). PRODIGY: A Contact-based Predictor of Binding Affinity in Protein-protein Complexes. *Bio Protoc* 7**,** e2124.

Watson, J.L., Juergens, D., Bennett, N.R., Trippe, B.L., Yim, J., Eisenach, H.E., Ahern, W., Borst, A.J., Ragotte, R.J., Milles, L.F., Wicky, B.I.M., Hanikel, N., Pellock, S.J., Courbet, A., Sheffler, W., Wang, J., Venkatesh, P., Sappington, I., Torres, S.V., Lauko, A., De Bortoli, V., Mathieu, E., Ovchinnikov, S., Barzilay, R., Jaakkola, T.S., Dimaio, F., Baek, M., and Baker, D. (2023). De novo design of protein structure and function with RFdiffusion. *Nature* 620**,** 1089-1100.

Weinberg, Z.Y., Soliman, S.S., Kim, M.S., Shah, D.H., Chen, I.P., Ott, M., Lim, W.A., and El-Samad, H. (2024). De novo-designed minibinders expand the synthetic biology sensing repertoire. *bioRxiv*.

Yang, W., Hicks, D.R., Ghosh, A., Schwartze, T.A., Conventry, B., Goreshnik, I., Allen, A., Halabiya, S.F., Kim, C.J., Hinck, C.S., Lee, D.S., Bera, A.K., Li, Z., Wang, Y., Schlichthaerle, T., Cao, L., Huang, B., Garrett, S., Gerben, S.R., Rettie, S., Heine, P., Murray, A., Edman, N., Carter, L., Stewart, L., Almo, S.C., Hinck, A.P., and Baker, D.

(2025). Design of high-affinity binders to immune modulating receptors for cancer immunotherapy. *Nat Commun* 16**,** 2001.